Long non-coding RNA OIP5-AS1 facilitates the progression of ovarian cancer via the miR-128-3p/CCNG1 axis

YUANYUAN LIU[1*], XIAOMIN FU[1*], XIUYUN WANG[1], YANLING LIU[2] and XIAOYAN SONG[2]

[1]Department of Obstetrics and Gynecology; [2]Ultrasound Department of Obstetrics and Gynecology, The Shengli Oilfield Central Hospital, Dongying, Shandong 257034, P.R. China

Received August 6, 2020; Accepted February 11, 2021

DOI: 10.3892/mmr.2021.12027

Abstract. Long non-coding RNA (LncRNA) o-phthalaldehyde-interacting protein 5 antisense transcript 1 (OIP5-AS1) serves major roles in the progression of various types of cancer. The present study investigated its biological function in ovarian cancer (OC) and its mechanisms. The levels of OIP5-AS1, microRNA-128-3p (miR-128-3p) and cyclin G1 (CCNG1) were examined by reverse transcription-quantitative PCR. Cell viability, apoptosis, migration and invasion were detected to analyze cellular progression. Glycolytic metabolism was assessed by detecting the levels of glucose consumption and lactate production. CCNG1 and hexokinase 2 protein levels were measured by western blotting. Dual-luciferase reporter assay, RNA immunoprecipitation and RNA pull-down assays were performed to affirm the interaction between two molecules. OIP5-AS1 was found to be upregulated in OC tissues and cells. Knockdown of OIP5-AS1 suppressed cell viability, migration, invasion and glycolysis while promoting apoptosis in OC cells. OIP5-AS1 interacted with miR-128-3p and functioned as an oncogene by sequestering miR-128-3p. In addition, CCNG1 was a target gene for miR-128-3p and miR-128-3p regulated the CCNG1-induced effects on OC cells by downregulating CCNG1. OIP5-AS1 upregulated the expression of CCNG1 via targeting miR-128-3p. OIP5-AS1 knockdown also inhibited tumor growth of OC *in vivo* by modulating the expression of miR-128-3p and CCNG1. Collectively, these data illustrated that the oncogenic role of OIP5-AS1 in OC was associated with the miR-128-3p/CCNG1 axis at least in part. OIP5-AS1 might be a probable diagnostic and therapeutic biomarker for the treatment of OC patients.

Correspondence to: Mrs. Xiaoyan Song, Ultrasound Department of Obstetrics and Gynecology, The Shengli Oilfield Central Hospital, 31 Jinan Road, Dongying, Shandong 257034, P.R. China
E-mail: zxyysxy01@163.com

*Contributed equally

Key words: long non-coding RNA o-phthalaldehyde-interacting protein 5 antisense transcript 1, ovarian cancer, microRNA-128-3p, cyclin G1

Introduction

Ovarian cancer (OC) is the seventh most common cancer among females with an estimated 239,000 new cases being diagnosed worldwide annually; the incidence rate (11.4 per 100,000) is the highest in Central and Eastern Europe (1). Although the diagnosis and treatment for OC have been increasingly successful, the 5-year survival rate of the advanced patient with OC is only ~30% (1,2). Therefore, it is imperative to search more molecular targets for promoting the diagnostic and therapeutic effects on OC patients. Studies have reported that long non-coding RNAs (lncRNAs) can regulate biological behaviors in OC cells (3-5).

Aerobic glycolysis, known as the 'Warburg effect', is characterized by oxidating glucose and producing lactate under the catalysis of diverse enzymes and normoxic conditions (6). Glycolysis can provide the energy for tumor cell growth and the promotion of glycolytic metabolism indicates the malignant progression of types of cancer (7). A number of lncRNAs have been shown to regulate the metabolic process of glycolysis in types of cancer, including OC (8-10). It may be pertinent to seek the useful targets in OC progression through the glycolytic metabolism. LncRNAs are common class of regulatory ncRNAs with length >200 nucleotides and lack of protein-encoding capacity (11).

LncRNAs can participate in the initiation and progression of various types of human tumors as oncogenes or tumor inhibitors (12,13). O-phthalaldehyde-interacting protein 5 antisense transcript 1 (OIP5-AS1) has been found as the regulator by acting as the sponges of microRNAs (miRNAs) in various types of cancers. For instance, Wang *et al* (14) revealed that OIP5-AS1 improves cell proliferation and results in poor prognosis through sponging miR-378a-3p in lung cancer. In addition, OIP5-AS1 knockdown restrains CCAAT/enhancer-binding protein α and TNF receptor-associated factor 4 levels to retard glioma cell growth via binding to miR-367-3p (15). OIP5-AS1 is reported to be overexpressed in OC and facilitates the malignant tumor growth and metastasis of OC by the miR-137/ZNF217 or miR-324-3p/NFIB axis (16,17). However, the regulation in glycolytic process of OC and other regulatory mechanisms underpinning OIP5-AS1 remain to be elucidated.

Non-coding miRNAs can cause mRNA degradation and translation inhibition by combining with the 3'-untranslated regions (3'-UTRs) of target mRNAs, leading to a significant

involvement in biological processes (18,19). Studies have found an inhibitory effect of miR-128-3p on the development of a number of carcinomas (20-22). The aberrant downregulation of miR-128 is found in OC (23,24). As a submit of miR-128, the present study hypothesized that miR-128-3p might also be associated with OC regulation.

Cyclin G1 (CCNG1), a member of cell cyclin protein, is dysregulated in leiomyoma and colorectal cancer (25,26). CCNG1 is associated with the regulation of miR-122a in hepatocellular carcinoma as a target of miR-122a (27). Studies also suggest that CCNG1 acts as an oncogene to enhance OC cell growth (28,29), but it is unknown if CCNG1 is a target of miR-128-3p in OC.

The present study was mainly devoted to investigating the role of OIP5-AS1 in OC and its functional mechanism with miR-128-3p and CCNG1, it also attempted to provide a novel pathogenesis for OC progression.

Materials and methods

Tissues acquisition and cell culture. A total of 41 patients with OC were recruited to this study between March 2015 and September 2018. A total of 41 paired tissues of OC and adjacent normal tissues (>3 cm from tumor sites) were acquired from these patients with OC (age range 18-60 years old) subjected to surgical excision in the Shengli Oilfield Central Hospital, after obtaining informed consents from the patients. These tissues were divided into two groups (I+II: n=23; III+IV: n=18) according to the tumor stage. All specimens were promptly stored in liquid nitrogen for subsequent RNA or protein extraction. The present study was approved and supported by the Shengli Oilfield Central Hospital.

Human ovarian surface epithelial cells (IOSE-80) and OC cell line OVCAR-3 were bought from American Type Culture Collection and another OC cell line, SKOV3, was obtained from the cell bank of the Chinese Academy of Sciences (Shanghai, China). These cells were cultured in basic medium RPMI 1640 (Invitrogen; Thermo Fisher Scientific, Inc.) complemented with 10% fetal bovine serum (FBS; Gibco; Thermo Fisher Scientific, Inc.) in a humidified incubator with a constant temperature of 37˚C and CO_2 concentration at 5%.

Cell transfection. Small interfering (si) RNA against OIP5-AS1 (si-OIP5-AS1, 5'-GGCTTTGTGTTCCTTATCACAGG-3'), siRNA against CCNG1 (si-CCNG1, 5'-TTGAAGTAAAAG ATCTTCTTAGT-3'), siRNA negative control (si-control, 5'-TTCTCCGAACGTGTCACGTTT-3'), short hairpin (sh) RNA vector against OIP5-AS1 (sh-OIP5-AS1, 5'-CCG GGCTCCTAGGATTCCAGTTATCCTCGAGGCAGAAGG CTGAGTTTCATTTTTTTTG-3'), shRNA vector negative control (sh-control, 5'-CACCGTTCTCCGAACGTGTCACGT CAAGAGATTACGTGACACGTTCGGAGAATTTTTTG-3'), miR-128-3p mimic (miR-128-3p, 5'-UCACAGUGAACC GGUCUCUUU-3'), mimic negative control (miR-control, 5'-UUGUACUACACAAAAGUACUG-3'), miR-128-3p inhibitor (anti-miR-128-3p, 5'-AAAGAGACCGGUUCACUG UGA-3'), inhibitor negative control (anti-control, 5'-CAGUAC UUUUGUGUAGUACAA-3') and the overexpression vector pCE-RB-Mam-OIP5-AS1 (OIP5-AS1) vector or the empty vector pCE-RB-Mam were all purchased from Guangzhou RiboBio Co., Ltd. Cell transfection was performed using Lipofectamine® 3000 (Invitrogen; Thermo Fisher Scientific, Inc.). Cells were seeded into the 24-well plates and cultured overnight to 50% coverage, then transfected with different concentrations of RNAs or vectors (40 nM siRNA, 40 nM shRNA vector, 40 nM mimic, 20 nM inhibitor or 2 μg pCE-RB-Mam/OIP5-AS1 vector). Further experimentation was performed after cells were incubated at 37˚C for 48 h.

RNA extraction and reverse transcription-quantitative (RT-q) PCR. The extraction of total RNA was performed using TRIzol® (Thermo Fisher Scientific, Inc.) from OC tissues and cells ($2x10^5$) in accordance with the manufacturer's protocol, followed by the quantification of RNA concentration. Then 1 μg RNA was reversely transcribed to synthesis the complementary DNA (cDNA) using Prime Script RT regent kit (Takara Bio, Inc.) according to the manufacturer's protocols. PCR reaction system was prepared in 384 well-plates using a TB Green Premix EX Taq II kit (Takara Bio, Inc.) following the manufacturer's protocol and amplified via ABI Step One Real-time PCR System (Thermo Fisher Scientific, Inc.). The reaction system was prepared on ice with a 20-μl volume: 10 μl TB Green Premix EX Taq II (2x), 0.8 μl forward primer, 0.8 μl reverse primer, 0.4 μl ROX Reference Dye, 2 μl cDNA, 6 μl sterile water. Three technical replications were set for each sample. The reaction protocols were as follows: Predenaturation at 95˚C for 30 sec, 40 cycles of denaturation at 95˚C for 5 sec and annealing at 60˚C for 30 sec. GAPDH and U6 were used as respective internal control for lncRNA or mRNA and miRNA. Primers were synthesized by Sangon Biotech Co., Ltd. and the sequences were: OIP5-AS1 (forward: 5'-TGCGAAGATGGCGGAGTAAG-3', reverse: 5'-TAGTTCCTCTCCTCTGGCCG-3'); miR-128-3p (forward: 5'-GCCGAGTCACAGTGAACCGGT-3', reverse: 5'-CAGTGCAGGGTCCGAGGTAT'); CCNG1 (forward: 5'-GTTACCGCTGAGGAGCTGCAGTC-3', reverse: 5'-ATAGCCATCATGGATAGACTCAG-3'); GAPDH (forward: 5'-GTCTCCTCTGACTTCAACAGCG-3', reverse: 5'- ACCACCCTGTTGCTGTAGCCAA-3'); U6 (forward: 5'-ATTGGAACGATACAGAGAAGATT-3', reverse: 5'-GGA ACGCTTCACGAATTTG-3'). The collected data from three independent experiments were analyzed using the $2^{-\Delta\Delta Cq}$ method (30).

3-(4, 5)-Dimethylthiazole-2-y1)-2, 5-biphenyl tetrazolium bromide (MTT) assay. Cell viability was examined by MTT assay. At 0, 24, 48 and 72 h post-transfection, 15 μl MTT solution (5 mg/ml, pH=7.4; Thermo Fisher Scientific, Inc.) was added to cells in the 96-well plates and incubated for another 4 h. Then the supernatants were slowly removed and 150 μl dimethylsulfoxide (DMSO; Thermo Fisher Scientific, Inc.) was added to each well for 10 min to resolve the generated formazan. The optical density (OD) value of each well at the wavelength of 490 nm was determined using a microplate reader (Thermo Fisher Scientific, Inc.).

Flow cytometry. An FITC Annexin V Apoptosis Detection kit I (BD Biosciences) was used to distinguish the apoptotic cells. After 48 h post-transfection, OVCAR-3 and SKOV3 cells were collected following digestion by 0.25% trypsin

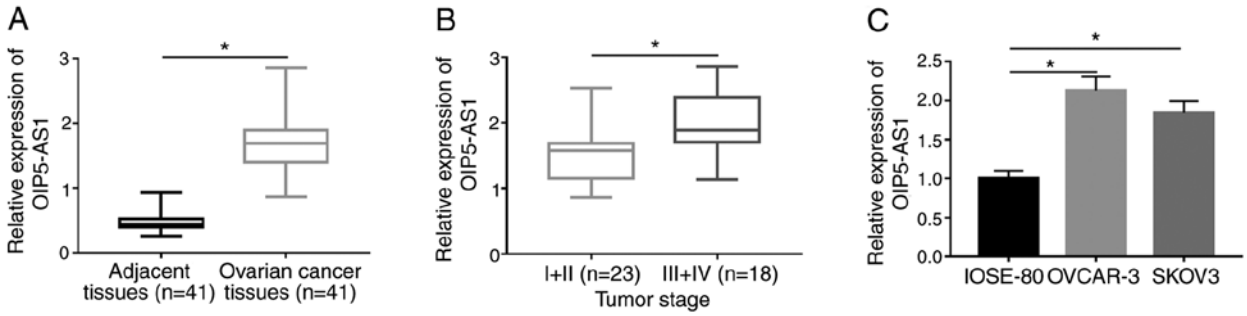

Figure 1. OIP5-AS1 was upregulated in OC tissues and cells. Reverse transcription-quantitative PCR was performed to analyze OIP5-AS1 expression in (A) OC tissues or adjacent normal tissues, (B) OC tissues at I+II or III+IV stages and (C) OC cell lines or normal cells. *P<0.05. OIP5-AS1, o-phthalaldehyde-interacting protein 5 antisense transcript 1; OC, ovarian cancer.

(GIBCO), then cell pellets were washed by pro-cooled phosphate buffered saline (PBS; GIBCO) and resuspended in 1X binding buffer. Afterwards, cells were stained by 5 μl FITC Annexin V and 5 μl PI for 15 min in the dark at room temperature according to the manufacturer's protocol. The apoptotic cells were examined using a BD Accuri C6 flow cytometer (BD Biosciences) and analyzed using the BD Accuri C6 system (32-bit) software (BD Biosciences). The apoptosis rate was calculated as the percentage of early apoptotic cells ($Annexin^+/PI^-$) and late apoptotic cells ($Annexin^+/PI^+$).

Transwell migration and invasion assays. A Transwell 24-well chamber (Corning Life Sciences) was used to detect the abilities of cell migration and invasion. Cell suspension in serum-free medium was pipetted into the upper chamber at room temperature. Simultaneously, 600 μl RPMI 1640 medium with 10% FBS was added to the lower chamber at room temperature. The chamber was incubated at 37˚C for 24 h, and cells that passed through the lower membranes were fixed with methyl alcohol (Sangon Biotech Co., Ltd.) for 10 min and stained with crystal violet (Sangon Biotech Co., Ltd.) for 10 min at room temperature. Finally, the cells were counted under an inverted light microscope (Olympus Corporation) and cell images were acquired at x100 magnification. For invasion assay, the lower surface of the upper chamber was coated with Matrigel (Corning Life Sciences) at 37˚C overnight before seeding the cells.

Detection of glucose consumption and lactate production. According to the manufacturer's protocol, the consumption of glucose and the production of lactate were assessed using glucose detection kit (cat. no. K188-200) and lactate detection kit (cat. no. K209-100) purchased from Beijing Zhonghao Biotechnology Co., Ltd.).

Western blotting assay. Total proteins from tissues and cells were extracted by RIPA Lysis Buffer (Sangon Biotech Co., Ltd.). The obtained proteins were quantified using BCA Protein Assay kit (Sangon Biotech Co., Ltd.) and 30 μg proteins were separated by sodium dodecyl sulfate polyacrylamide gel electrophoresis (SDS-PAGE) on 10% gels for 2 h. Next, the separated proteins were transferred onto the polyvinylidene fluoride (PVDF) membranes (Thermo Fisher Scientific, Inc.). These membranes were then immersed in 5% skimmed milk (Sangon Biotech Co., Ltd.) diluted with phosphate buffered saline and 0.1% Tween 20 (PBST) at room temperature for 3 h to prevent the non-specific protein binding, followed by incubation with primary antibodies overnight at 4˚C. The primary antibodies were: anti-hexokinase 2 (anti-HK2; Abcam; cat. no. ab209847; 1:1,000), anti-CCNG1 (Abcam; cat. no. ab170389; 1:1,000) and anti-β-actin (Abcam; cat. no. ab8227; 1:3,000). Finally, the chromogenic reaction was performed by an HRP/DAB (ABC) detection kit (Abcam) after the incubation of anti-rabbit secondary antibody (Abcam; cat. no. ab205718; 1:5,000) for 1 h at room temperature. The gray level of each band was obtained by the statistical analysis of ImageJ software (National Institutes of Health) using β-actin as the endogenous reference.

Dual-luciferase reporter assay. The online software applications StarBase (http://starbase.sysu.edu.cn) and TargetScan (http://www.targetscan.org) were used to seek the miRNA target of OIP5-AS1 and target gene for miR-128-3p, respectively. To construct the recombinant luciferase plasmids, the wild-type (WT) OIP5-AS1 and 3'UTR of CCNG1 sequences were respectively cloned into the pGL-3 luciferase basic vector (Promega Corporation) to acquire WT-OIP5-AS1 and WT-CCNG1, then their mutant-types (MUT) with the mutant sites for miR-128-3p were also constructed as MUT-OIP5-AS1 and MUT-CCNG1. Each constructed luciferase reporter plasmid was transfected into OVCAR-3 and SKOV3 cells with miR-128-3p or miR-control by Lipofectamine 3000. After transfection for 48 h, cells were lysed and the luciferase intensity was determined by the dual-luciferase reporter system (Promega Corporation) following the manufacturer's protocol. The luciferase activity ratio of firefly and *Renilla* was considered to be the relative luciferase activity.

RNA immunoprecipitation (RIP) assay. RIP assay was performed using Magna RNA immunoprecipitation kit (EMD Millipore). OC cells were centrifuged at 4˚C and 16,000 x g for 10 min and $2x10^7$ cells were lysed using RIPA lysis buffer (EMD Millipore). The cells were then incubated with magnetic beads pro-covered with antibodies against Argonaute2 (Anti-Ago2; Abcam; cat. no. ab32381) using anti-Immunoglobulin G (Anti-IgG; Abcam; cat. no. ab205718) as the negative reference. RNA was extracted using TRIzol

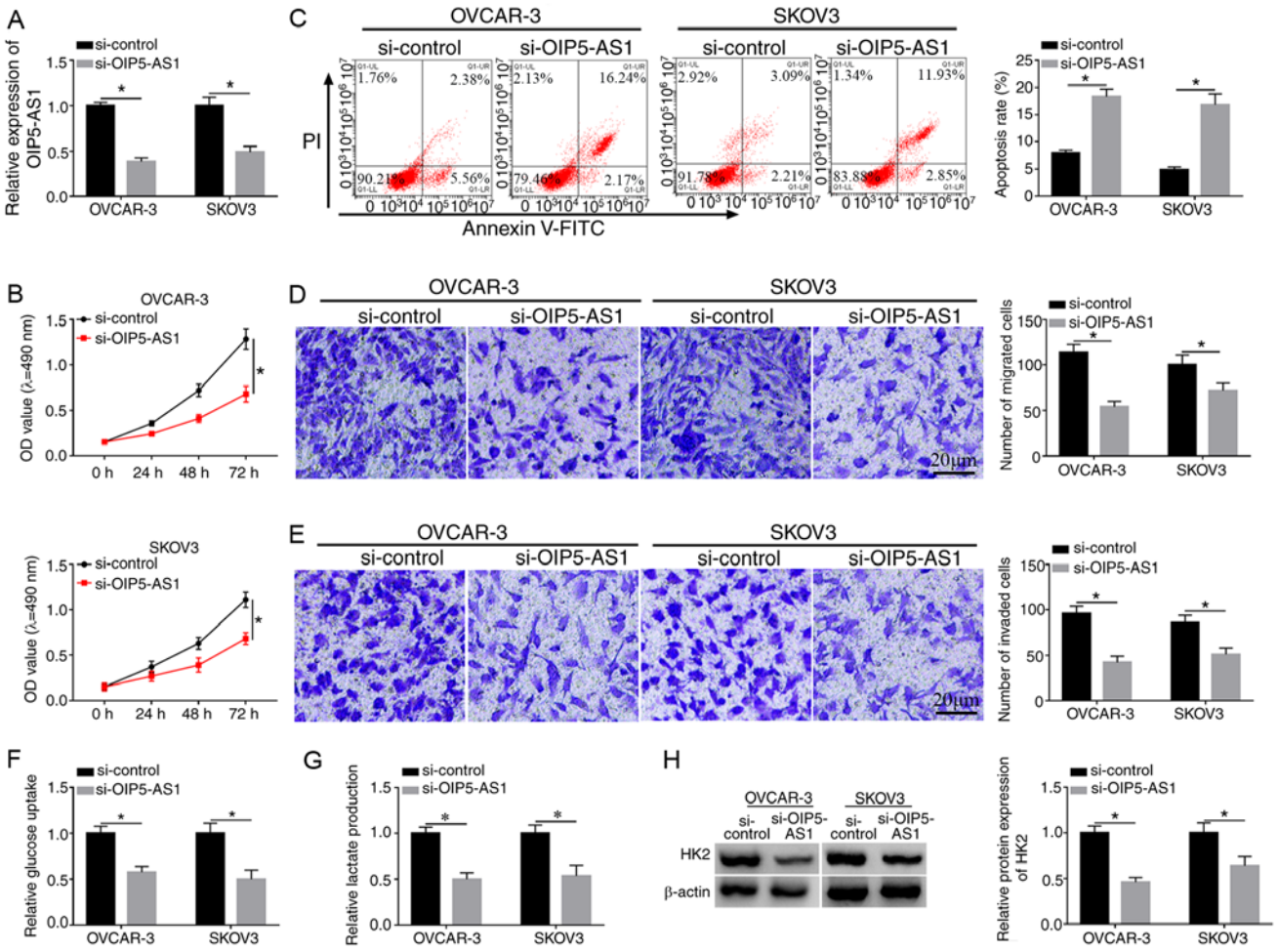

Figure 2. Knockdown of OIP5-AS1 represses cell viability, migration, invasion and glycolysis while promoting apoptosis in OC cells. (A) The knockdown efficiency of si-OIP5-AS1 was detected by reverse transcription-quantitative PCR. (B) MTT assay was used to examine cell viability. (C) Flow cytometry was exploited to determine cell apoptosis rate. Transwell assay was used to measure cell (D) migration and (E) invasion abilities. (F) Glucose consumption and (G) lactate production were evaluated by glucose detection and lactic acid detection kits. (H) Western blotting was employed to detect the protein expression of HK2. *P<0.05. OIP5-AS1, o-phthalaldehyde-interacting protein 5 antisense transcript 1; OC, ovarian cancer; si-, small interfering; HK2, hexokinase 2.

and the RNA enrichment was detected via RT-qPCR. Finally, the levels of OIP5-AS1 and miR-128-3p in Anti-IgG and Anti-Ago2 groups were compared.

RNA pull-down assay. Pierce™ Biotinylated Protein Interaction Pull-Down kit (Thermo Fisher Scientific, Inc.) was used to perform the pull-down assay. OVCAR-3 and SKOV3 cells were transfected with biotin-labeled miR-128-3p (Bio-miR-128-3p) or Bio-NC (Guangzhou RiboBio Co., Ltd) using Lipofectamine 3000. Following transfection at 37˚C for 48 h, cells were harvested by centrifugation at 4˚C and 16,000 g for 10 min. The cell lysates were then incubated with streptavidin-coupled agarose beads at 4˚C overnight. Following the isolation of RNA from the washed beads by TRIzol, the enrichment of OIP5 was measured by RT-qPCR analysis.

Xenograft tumor assay. A total of 12 BALB/c nude mice (six-week-old, 20-25 g) were purchased from Beijing Vital River Laboratory Animal Technology Co., Ltd. and maintained in a specific-pathogen-free environment under temperature of 25˚C, humidity of 70% and a 12 h light/dark cycle. These mice received food and water *ad libitum*. Mice were arbitrarily divided into two groups with 6 mice/group, comprising sh-control and sh-OIP5-AS1 groups. The xenograft tumor model was established through the subcutaneous injection of $2x10^6$ OVCAR-3 cells stably expressed sh-OIP5-AS1 or sh-control into the left flank of mouse's back. The health and behavior of mice were monitored every 2 days and tumor volume (length x $width^2$ x 0.5) was measured using a digital caliper every week. After cell injection for 4 weeks, tumor volume reached 900 mm^3 (<1,000 mm^3, which was set as the humane endpoint) and the mice were sacrificed. The 30% air of environment (per min) was displaced using the flow rate of CO_2 according to the current guidelines of the American Veterinary Medical Association (31), then mice were verified to have succumbed by monitoring the breathing. No mice died during the 4-week experimental period. The tumor tissues were excised from mice and weighed on an electronic scale. The examination of OIP5-AS1, miR-128-3p and CCNG1 was performed via RT-qPCR or western blotting. This experiment was ratified by the Animal Ethics Committee of the Shengli Oilfield Central Hospital and all procedures followed the guidelines

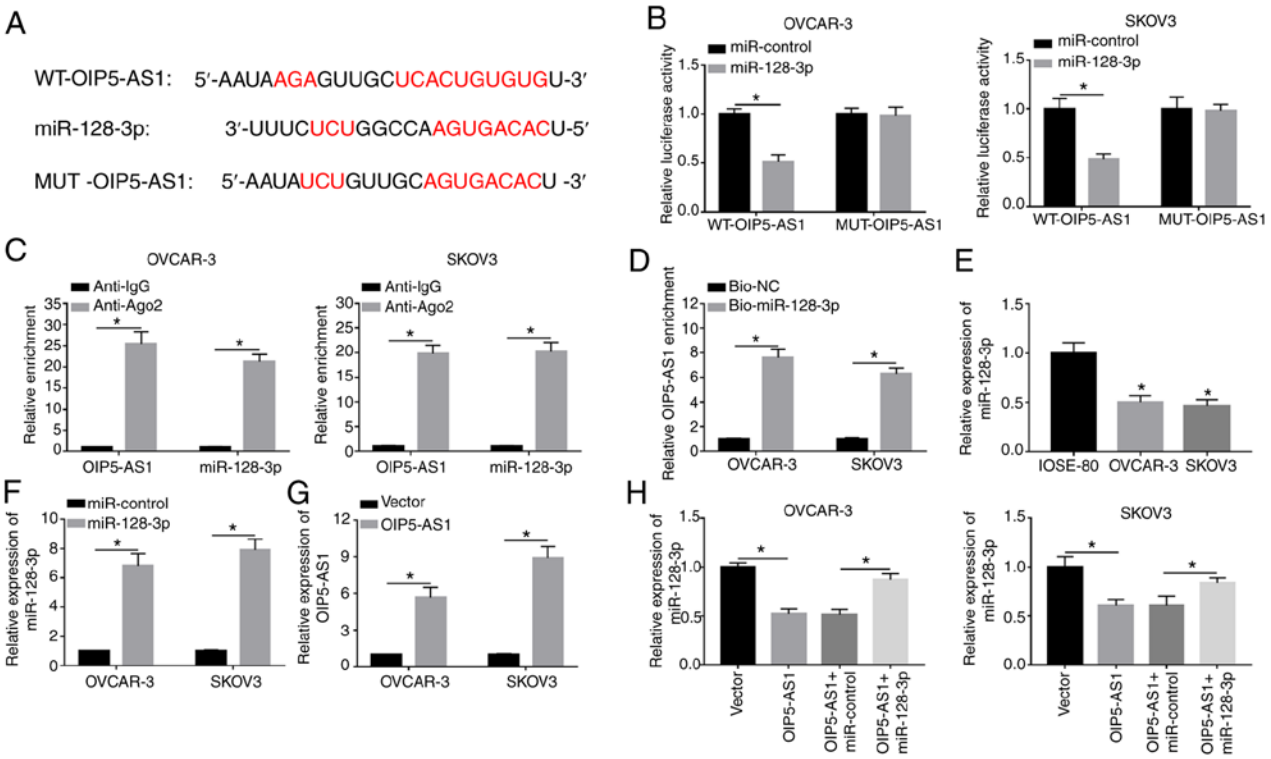

Figure 3. OIP5-AS1 interacts with miR-128-3p. (A) StarBase software was used to predict the potential miRNA target of OIP5-AS1. The combination between OIP5-AS1 and miR-128-3p was verified by (B) dual-luciferase reporter assay, (C) RNA immunoprecipitation and (D) RNA pull-down assay. (E) The expression of miR-128-3p was detected by RT-qPCR in OC cells. RT-qPCR was performed to determine the overexpression effects of (F) miR-128-3p and (G) OIP5-AS1. (H) Following transfection of OIP5-AS1, OIP5-AS1 + miR-128-3p or relative controls in OC cells, miR-128-3p level was determined by RT-qPCR. *P<0.05. OIP5-AS1, o-phthalaldehyde-interacting protein 5 antisense transcript 1; miR, microRNA; RT-qPCR, reverse transcription-quantitative PCR; OC, ovarian cancer.

provided by the National Institutes of Health for the Care and Use of Laboratory Animals, 8th edition (32).

Statistical analysis. All data were given as the mean ± standard deviation from three independent experiments. SPSS 19.0 (IBM Corp.) was used to conduct statistical analysis and figure plotting was performed using GraphPad Prism 7 (GraphPad Software, Inc.). The differences of two groups and more than two groups were analyzed through Student's t-test and a one-way analysis of variance followed by Tukey's post hoc test. P<0.05 was considered to indicate a statistically significant difference.

Results

OIP5-AS1 is upregulated in OC tissues and cells. RT-qPCR analysis was firstly conducted to examine the expression of OIP5-AS1. OIP5-AS1 expression was markedly increased in OC tissues compared with the adjacent normal tissues (Fig. 1A). Among 41 OC tissues, OIP5-AS1 was upregulated in tissues at III+IV stage compared with those tissues at I+II stage (Fig. 1B). OIP5-AS1 expression was higher in both OVCAR-3 and SKOV3 cells compared with normal human ovarian IOSE-80 cells (Fig. 1C). This dysregulation of OIP5-AS1 implied its vital role in OC.

Knockdown of OIP5-AS1 represses cell viability, migration, invasion and glycolysis while promoting apoptosis in OC cells. OVCAR-3 and SKOV3 cells were transfected with si-OIP5-AS1 or si-control to investigate the function of OIP5-AS1 in OC. As shown in Fig. 2A, the decreased OIP5-AS1 expression in si-OIP5-AS1 group compared with the si-control group demonstrated that OIP5-AS1 was successfully knocked down in the two cell lines. MTT assay demonstrated that cell viabilities of OVCAR-3 and SKOV3 cells were distinctly reduced following the introduction of si-OIP5-AS1 compared with si-control group (Fig. 2B), while the apoptosis rate was shown to be increased (Fig. 2C). Transwell assay suggested that the migrated and invaded cells were decreased after downregulation of OIP5-AS1 (Fig. 2D and E). Analysis of glycolysis was performed by the detection of glucose consumption and lactate production, as well as the protein level of HK2 (an important enzyme of glycolysis). The data revealed that the transfection of si-OIP5-AS1 suppressed the consumption of glucose (Fig. 2F), lactate production (Fig. 2G) and HK2 protein expression (Fig. 2H) in both OVCAR-3 and SKOV3 cells, indicating that OIP5-AS1 knockdown caused the inhibition of glycolysis. These results suggested that knockdown of OIP5-AS1 repressed the progression of OC.

OIP5-AS1 interacts with miR-128-3p. LncRNAs exert their regulatory effects through sponging miRNAs generally (33). As demonstrated in Fig. 3A, StarBase predicted that OIP5-AS1 contained the binding sequences (UCACUGUG) for miR-128-3p and these sites were mutated into AGUGACAC in mutant OIP5-AS1. After performing the dual-luciferase reporter assay, it was found that the luciferase activity of WT-OIP5-AS1 plasmid was definitely inhibited by miR-128-3p

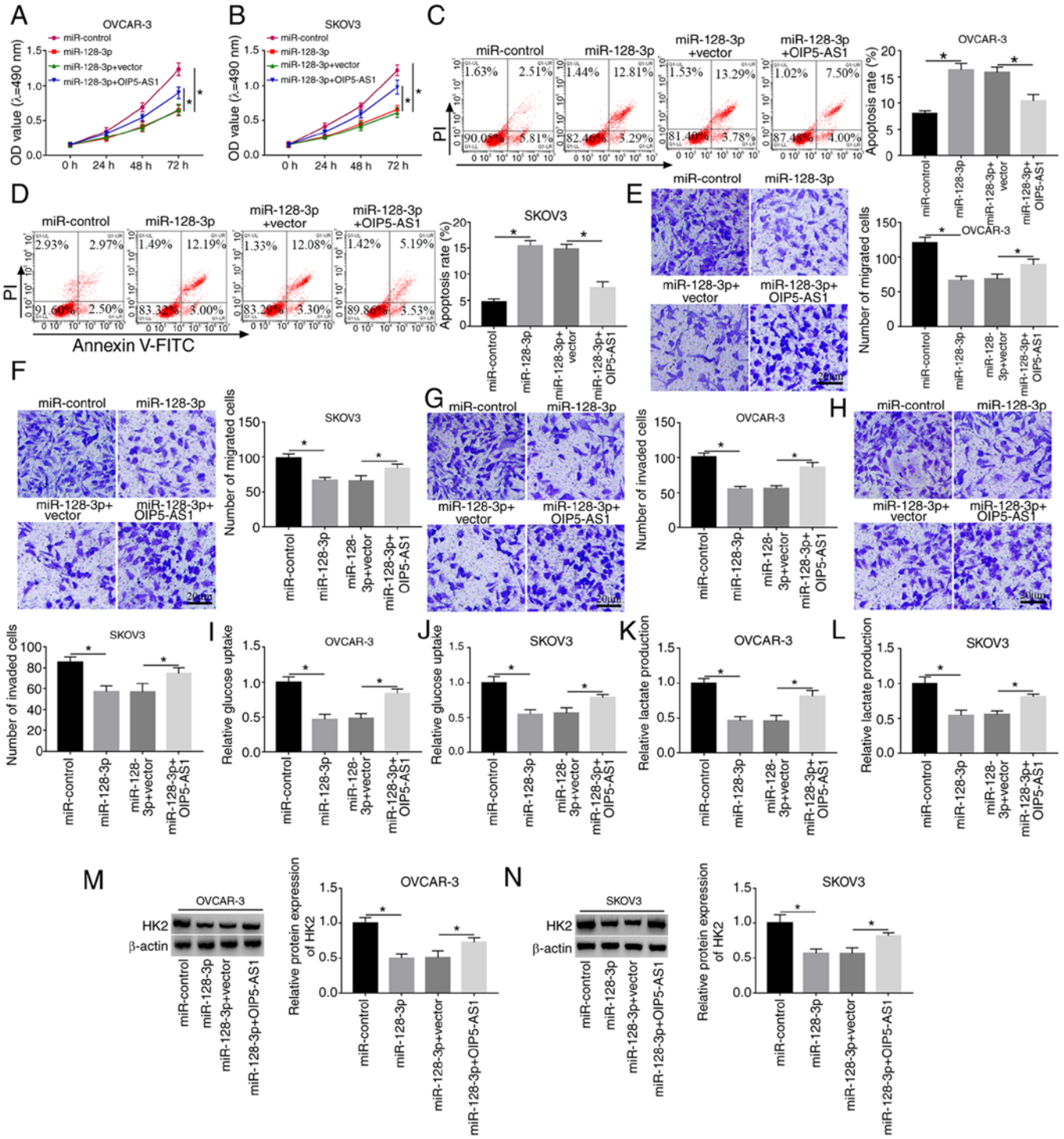

Figure 4. Overexpression of OIP5-AS1 ameliorates the suppressive effects of miR-128-3p on the progression of OC cells. MTT assay was performed to analyze cell viability in (A) OVCAR-3 and (B) SKOV3 cells transfected with miR-128-3p, miR-128-3p + OIP5-AS1 or matched controls. (C and D) The assessment of apoptosis was performed using Annexin V/PI flow cytometry. The evaluation of cell migration (E and F) and (G and H) invasion was performed via Transwell assay. Glucose detection and lactic acid detection kits were administrated for measuring (I and J) glucose consumption and (K and L) lactate production. (M and N) The detection of HK2 was conducted by western blotting. *P<0.05. OIP5-AS1, o-phthalaldehyde-interacting protein 5 antisense transcript 1; miR, microRNA; OC, ovarian cancer; HK2, hexokinase 2.

mimic (compared with the miR-control group) while there was no obvious change in MUT-OIP5-AS1 group of OVCAR-3 and SKOV3 cells (Fig. 3B). RIP assay demonstrated that OIP5-AS1 and miR-128-3p were enriched in Ago-2 pellet compared with the IgG group (Fig. 3C). Moreover, the enrichment of OIP5-AS1 was much higher in Bio-miR-128-3p group compared with the Bio-NC group, suggesting that OIP5-AS1 was pulled down by miR-128-3p (Fig. 3D). Subsequently, the miR-128-3p expression in OC cells was examined and the results indicated that miR-128-3p level was downregulated in OVCAR-3 and SKOV3 cells compared with normal IOSE-80 cells (Fig. 3E). After verifying the successful overexpression effects on miR-128-3p

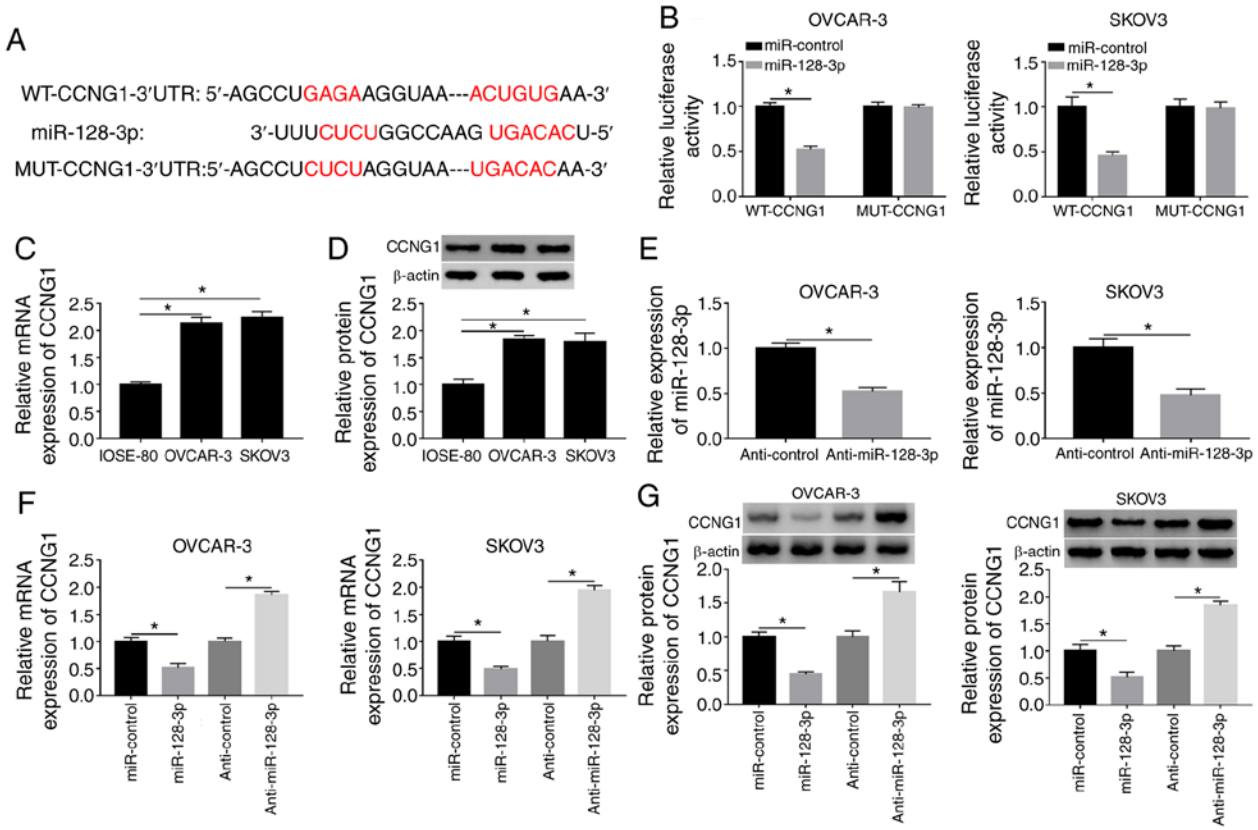

Figure 5. CCNG1 is a target of miR-128-3p. (A) The potential target of miR-128-3p was predicted by TargetScan software. (B) The relationship between miR-128-3p and CCNG1 was explored by the dual-luciferase reporter assay. The mRNA and protein expression levels of CCNG1 were determined by (C) RT-qPCR and (D) western blotting assays in OC cells. (E) The inhibitory effect of anti-miR-128-3p on miR-128-3p level was assayed by RT-qPCR. The determination of CCNG1 was performed by (F) RT-qPCR and (G) western blotting in OVCAR-3 and SKOV3 cells transfected with miR-128-3p, anti-miR-128-3p or the respective controls. *P<0.05. CCNG1, cyclin G1; miR, microRNA; RT-qPCR, reverse transcription-quantitative PCR; WT, wild-type; MUT, mutant-type.

and OIP5-AS1 by miR-128-3p mimic and OIP5-AS1 vector (Fig. 3F and G), it was noticed that miR-128-3p overexpression could recover the OIP5-AS1-induced miR-128-3p suppression (Fig. 3H). The results demonstrated that OIP5-AS1 could directly sponge miR-128-3p.

Overexpression of OIP5-AS1 ameliorates the suppressive effects of miR-128-3p on the progression of OC cells. To explore the regulatory mechanism of OIP5-AS1 and miR-128-3p, OVCAR-3 and SKOV3 cells were transfected with miR-128-3p, miR-128-3p+OIP5-AS1 or their matched controls. MTT and flow cytometry demonstrated that miR-128-3p had a suppressive effect on cell viability (Fig. 4A and B) and a promoting effect on apoptosis (Fig. 4C and D) in OVCAR-3 and SKOV3 cells, whereas the overexpression of OIP5-AS1 reversed these effects. Cell migration (Fig. 4E and F) and invasion (Fig. 4G and H) were inhibited by miR-128-3p transfection, which was abrogated following the upregulation of OIP5-AS1. OIP5-AS1 transfection counteracted the inhibition of glucose consumption (Fig. 4I and J) and lactate production (Fig. 4K and L) caused by miR-128-3p. The miR-128-3p-induced downregulation of HK2 protein level was clearly alleviated by the promotion of OIP5-AS1 expression (Fig. 4M and N). Hence, the inhibitory effect of miR-128-3p on OC progression was abated by OIP5-AS1 overexpression.

CCNG1 is a target of miR-128-3p. TargetScan software predicted the binding domain of miR-128-3p in the 3'-UTR sequence of CCNG1 (Fig. 5A), indicating that CCNG1 might be a potential target of miR-128-3p. Dual-luciferase reporter assay proved the combination of miR-128-3p and CCNG1 because the overexpression of miR-128-3p markedly repressed the luciferase activity of WT-CCNG1 group but failed to decrease that of MUT-CCNG1 group (Fig. 5B). Then RT-qPCR and western blotting revealed that the mRNA and protein expression levels of CCNG1 were higher in OVCAR-3 and SKOV3 cells than those in normal IOSE-80 cells (Fig. 5C and D). The RT-qPCR analysis showed that the repressive impact of anti-miR-128-3p on the expression of miR-128-3p was significant (Fig. 5E). Subsequently, the introduction of miR-128-3p was presented to suppress the CCNG1 mRNA and protein levels, while the opposite effects were observed following anti-miR-128-3p transfection (Fig. 5F and G). Collectively, miR-128-3p directly targeted CCNG1.

Downregulation of miR-128-3p restored the si-CCNG1-induced effects on OC cells. To explore whether CCNG1 was associated with the influence of miR-128-3p on OC development, transfection of si-CCNG1, si-CCNG1 + anti-miR-128-3p or the relative controls was conducted in OVCAR-3 and SKOV3 cells. Western blotting indicated that si-CCNG1 transfection markedly decreased the protein level of CCNG1, while

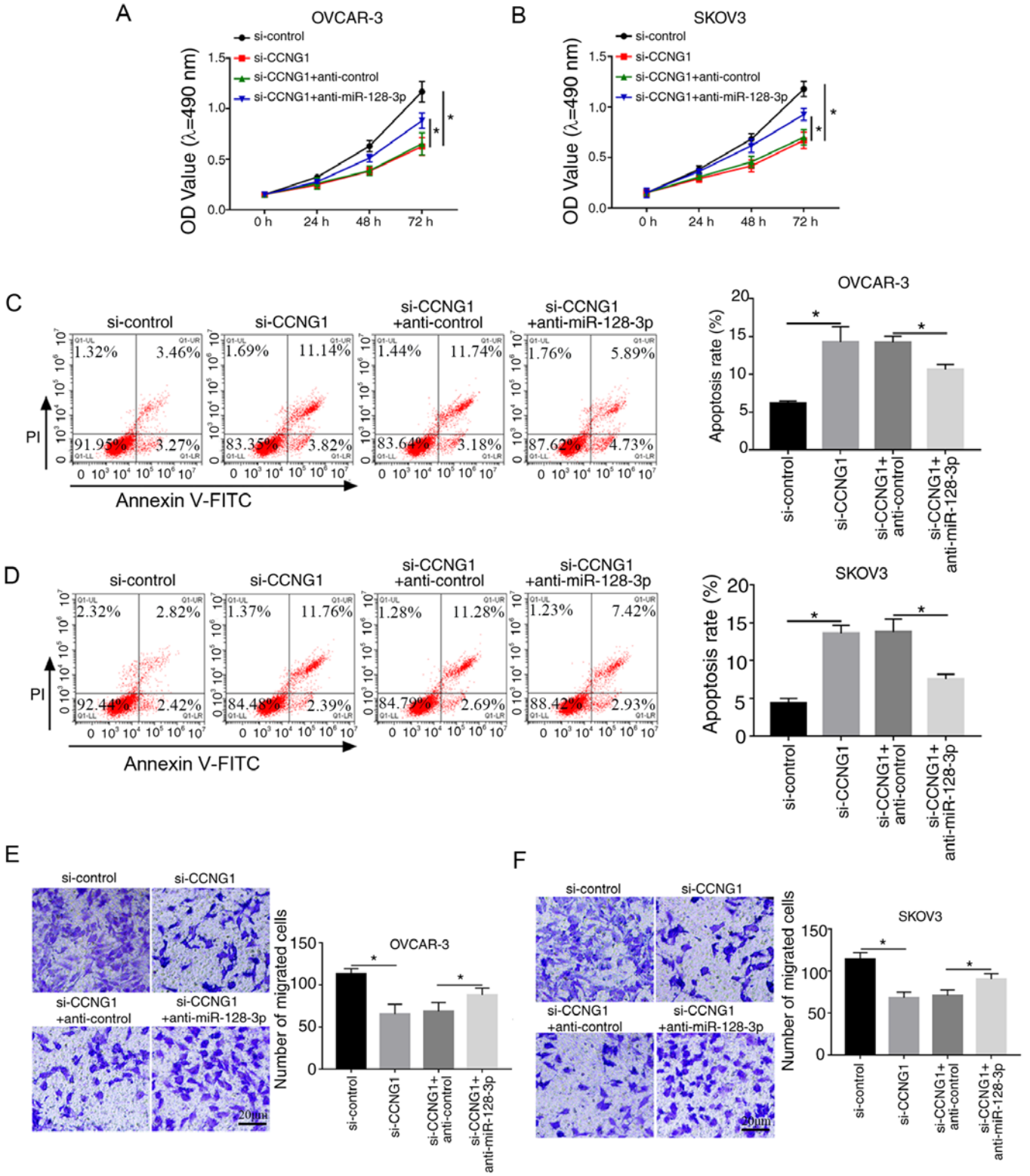

Figure 6. Continued.

miR-128 inhibitor relieved this expression downregulation in OVCAR-3 and SKOV3 cells (Fig. S1). Subsequent experiments demonstrated that anti-miR-128-3p partly abolished the si-CCNG1-induced cell viability repression (Fig. 6A and B), apoptosis enhancement (Fig. 6C and D) and migration (Fig. 6E and F) or invasion (Fig. 6G and H) inhibition. Additionally, the decline of glucose consumption (Fig. 6I and J), lactate production (Fig. 6K and L) and HK2 protein level (Fig. 6M and N) caused by CCNG1 knockdown was also weakened following the downregulation of miR-128-3p. Above data clarified that miR-128-3p inhibition lightened the effects of CCNG1 knockdown on OC cells, hinting that CCNG1 inhibition was responsible for the anti-cancer effect of miR-128-3p on OC.

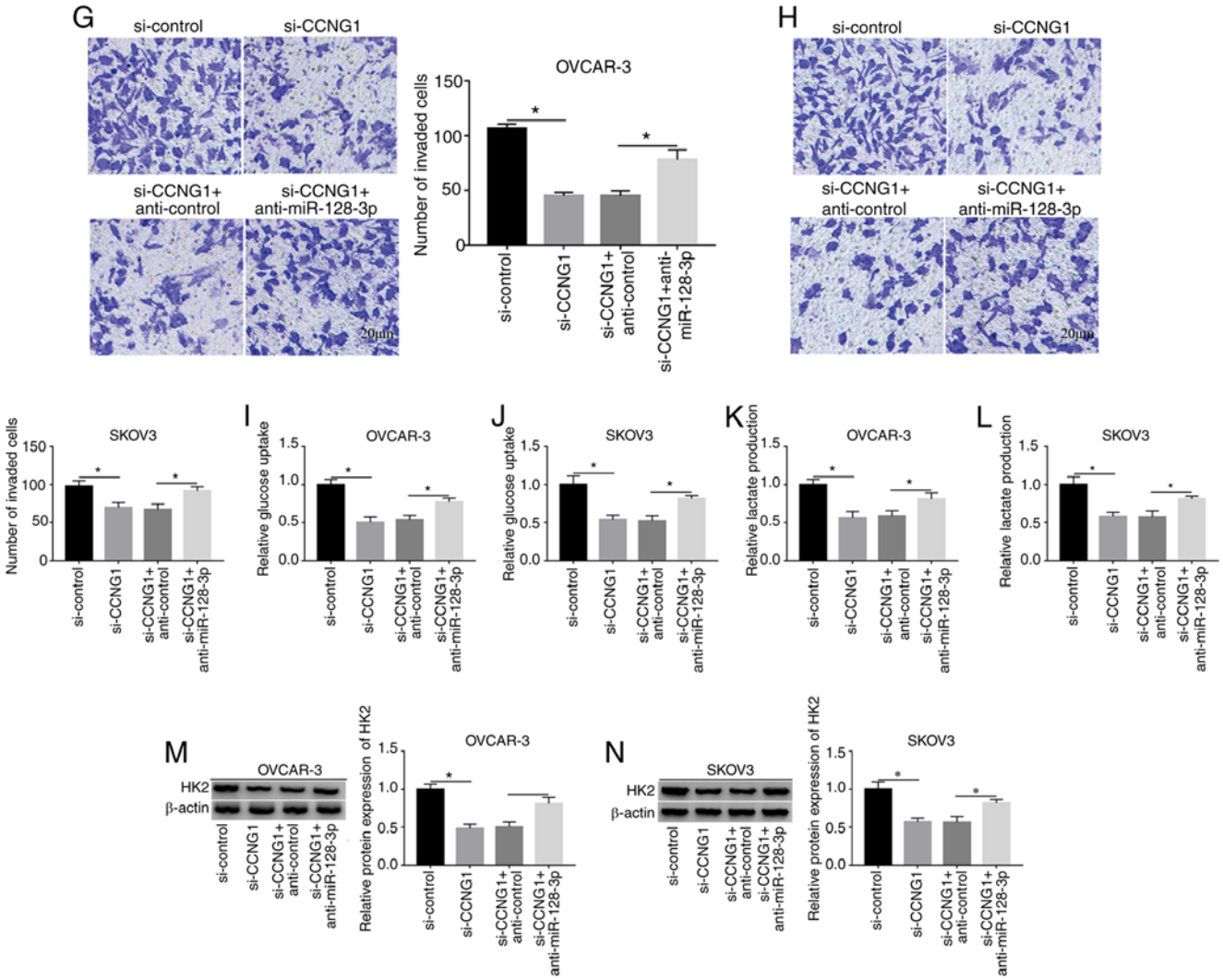

Figure 6. Downregulation of miR-128-3p restored the si-CCNG1-induced effect on OC cells. (A and B) Cell viability was examined by MTT assay after transfection of si-CCNG1, si-CCNG1+anti-miR-128-3p or the corresponding controls. (C and D) Cell apoptosis was detected by flow cytometry. (E and F) Cell migration and (G and H) invasion were measured by Transwell assay. The examination of (I and J) glucose consumption and (K and L) lactate production was performed via glucose detection and lactic acid detection kits. (M and N) The protein expression of HK2 was determined by western blotting assay. *P<0.05. miR, microRNA; si-, small interfering; CCNG1, cyclin G1; OC, ovarian cancer; HK2, hexokinase 2.

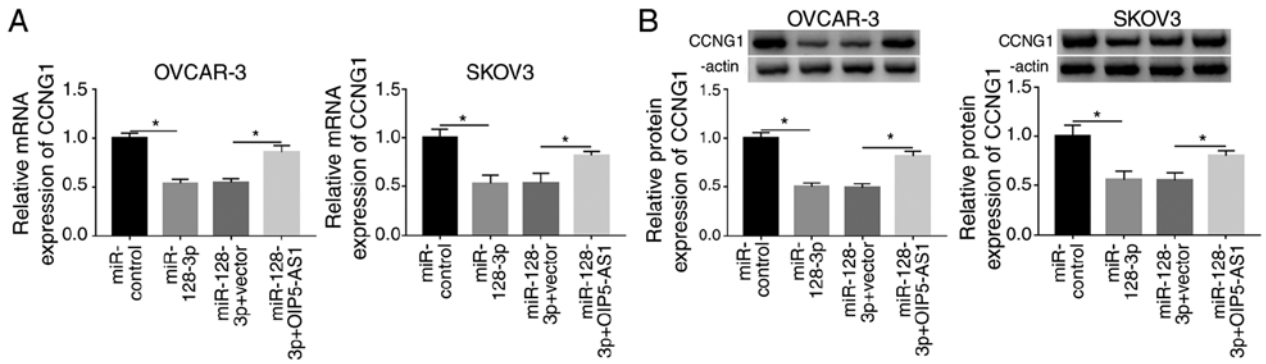

Figure 7. OIP5-AS1 upregulates CCNG1 expression via sponging miR-128-3p in OC cells. (A) mRNA and (B) protein expression of CCNG1 was measured by reverse transcription-quantitative PCR and western blotting in OVCAR-3 and SKOV3 cells transfected with miR-128-3p, miR-128-3p + OIP5-AS1 or their relative controls. *P<0.05. OIP5-AS1, o-phthalaldehyde-interacting protein 5 antisense transcript 1; CCNG1, cyclin G1; miR, microRNA; OC, ovarian cancer.

OIP5-AS1 upregulated CCNG1 expression via sponging miR-128-3p in OC cells. To ascertain whether CCNG1 could be regulated by OIP5-AS1, OVCAR-3 and SKOV3 cells were respectively transfected with miR-control, miR-128-3p, miR-128-3p+vector or miR-128-3p+OIP5-AS1, followed by the analysis of RT-qPCR and western blotting. As shown in

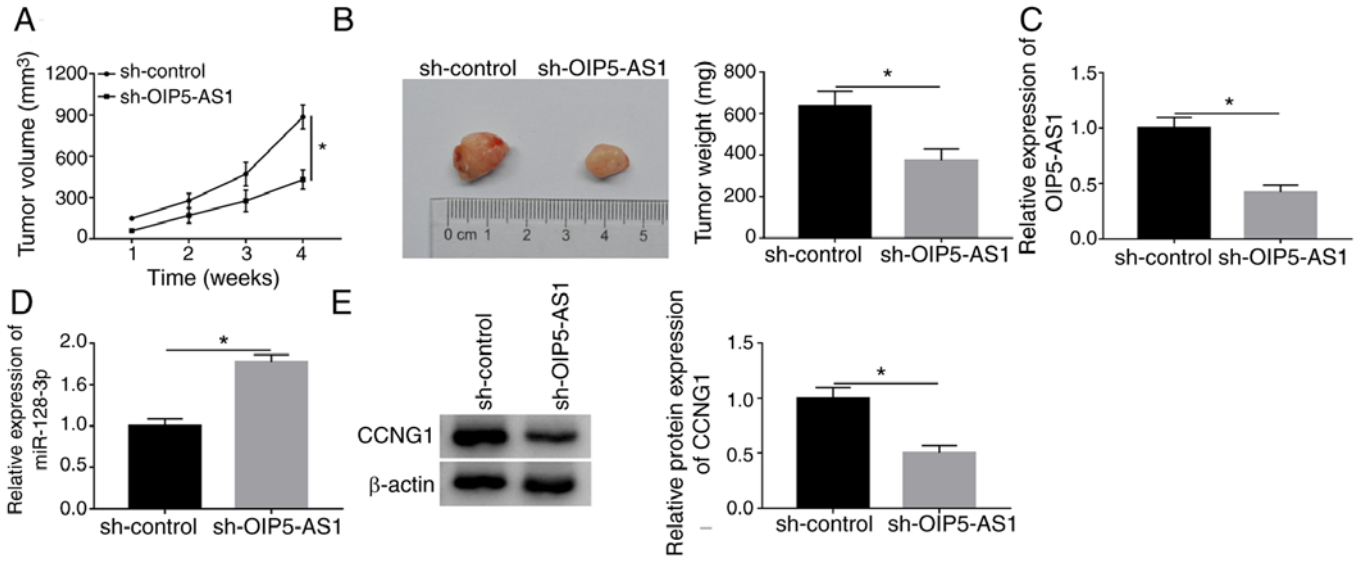

Figure 8. OIP5-AS1 depression inhibited tumor growth of OC by miR-128-3p/CCNG1 axis *in vivo*. (A) Tumor volume and (B) weight were measured in sh-OIP5-AS1 and sh-control groups. (C) The levels of OIP5-AS1 and (D) miR-128-3p were examined using reverse transcription-quantitative PCR. (E) CCNG1 protein expression was measured using western blotting. *P<0.05. OIP5-AS1, o-phthalaldehyde-interacting protein 5 antisense transcript 1; OC, ovarian cancer; miR, microRNA; sh-, short hairpin; CCNG1, cyclin G1.

Fig. 7A and B, miR-128-3p transfection resulted in reducing the CCNG1 mRNA and protein levels, which was ameliorated by ectopic high expression of OIP5-AS1. In sum, OIP5-AS1 could upregulate the CCNG1 level by targeting miR-128-3p.

OIP5-AS1 depression inhibited tumor growth of OC by miR-128-3p/CCNG1 axis in vivo. The xenograft tumor model was constructed to explore the effect of OIP5-AS1 on OC *in vivo*. As Fig. 8A and B demonstrate, tumor volume and weight were significantly lower in sh-OIP5-AS1 group compared with the sh-control group, implying that OIP5-AS1 knockdown restrained the OC carcinogenesis *in vivo*. In contrast to the sh-control group, the expression of OIP5-AS1 was downregulated (Fig. 8C) but miR-128-3p was upregulated (Fig. 8D) in sh-OIP5-AS1 group according to the results of RT-qPCR. CCNG1 protein level was decreased with the downregulation of OIP5-AS1 in western blot assay (Fig. 8E). Therefore, OIP5-AS1 knockdown impeded the oncogenesis of OC by the miR-128-3p/CCNG1 axis *in vivo*.

Discussion

OC is one of the most common and familiar diseases of the reproductive system with an estimated 239,000 new cases being diagnosed worldwide annually (1), which can lead to the severe injury and mortality. Present clinical therapies leave much to be desired due to the dissatisfactory outcomes for OC patients. In recent years, lncRNAs have been reported to participate in regulating various types of cancers, including OC (34,35). In the present study, OIP5-AS1 was considered as a diagnostic and therapeutic biomarker in OC and the OIP5-AS1/miR-128-3p/CCNG1 network was revealed.

A previous study, using the analysis of The Cancer Genome Consortium, suggested that OIP5-AS1 was overexpressed in human epithelial origin types of cancer, including lung, cervical and head and neck tumors (36). Consistent with this finding, the present study also found that the expression of OIP5-AS1 in OC tissues and cells was conspicuously upregulated. It has been reported that the proliferation and migration of glioma cells are inhibited after OIP5-AS1 knockdown (37). In addition, a study of cervical cancer revealed that silencing OIP5-AS1 reduced cell proliferation of HeLa cells (38). Bai and Li (39) stated that cell proliferation and migration were impeded, while more apoptotic cells were induced, following the silence of OIP5-AS1 in gastric cancer. Knockdown of OIP5-AS1 restrained cell viability, migration, invasion and induced apoptosis in OC cells during the current study, which agrees with the results of OIP5-AS1 in other OC research (16,17). The link between OIP5-AS1 and glycolysis has yet to be reported. The present study revealed the inhibitory effects of low OIP5-AS1 expression on glucose consumption, lactate production and HK2 level. The acceleration of glycolysis by OIP5-AS1 also reflected its oncogenic function in OC evolution.

Previous studies have reported that lncRNAs can inhibit miRNA activity as miRNA 'sponges' (40-42). OIP5-AS1 is reported to interact with miRNAs in different types of cancer, such as lung cancer and glioma (14,15). In the present study, miR-128-3p was identified as a target of OIP5-AS1 and OIP5-AS1 was involved in the cellular processes of OC by sponging miR-128-3p. Sun *et al* (43) found that OIP5-AS1 regulates Wnt-7b expression via targeting miR-410 in glioma cells. Nevertheless, the target of miR-128-3p in OC cells remains to be elucidated. Glycolytic metabolism has been found to be associated with G1/S transition in cell cycle progression of types of cancer (44,45). In 1996, Horne *et al* (46) first discovered the high expression of CCNG1 in skeletal muscle, kidney and ovary. Knockdown of CCNG1 can reduce the incidence of hepatic tumor (47). The present study found that downregulating CCNG1 repressed cell growth, migration, invasion and glycolysis, demonstrating the pro-cancer effect of CCNG1 on OC. Subsequently, CCNG1 was reported to promote OC progression as the target genes of miR-1271 and

miR-23b (28,29). The data of the present study proved that CCNG1 functioned as a downstream target of miR-128-3p and the role of miR-128-3p in OC was attributed to the negative regulation of CCNG1.

Notably, OIP5-AS1 has already been proved to modulate glioma progression through the miR-410/Wnt-7b axis (43). The results of the present study clearly indicated that OIP5-AS1 indirectly regulated the CCNG1 level by sponging miR-128-3p. The oncogenic role of OIP5-AS1 in OC was achieved by the regulatory network of miR-128-3p/CCNG1. Furthermore, the xenograft tumor assay also demonstrated that the carcinogenic effect of OIP5-AS1 in OC was dependent on the miR-128-3p/CCNG1 axis *in vivo*.

There are certain limitations to the current study. First, the effects of OIP5-AS1/miR-128-3p/CCNG1 on several signaling pathways remain to be elucidated. Second, other targets of miR-128-3p associated with glycolysis need to be discovered. Given the involvement of OIP5-AS1 and miR-128-3p in glycolytic metabolism, it would be worth exploring the potentials of glycolytic genes including phosphoglycerate dehydrogenase and glucose 6-phosphatase as the targets of miR-128-3p.

In conclusion, the present study revealed that OIP5-AS1 worked as a tumorigenic factor in OC development via the miR-128-3p/CCNG1 axis and revealed the OIP5-AS1/miR-128/CCNG1 modulatory network in OC. The present study might lay the foundation for OC progression at the lncRNA level.

Acknowledgements

Not applicable.

Funding

No funding was received.

Availability of data and materials

The analyzed data sets generated during the present study are available from the corresponding author on reasonable request.

Authors' contributions

XF and XW were responsible for the conceptualization and methodology; YaL, YuL and XS performed formal analysis and data curation; YuL and YaL were responsible for validation and investigation; and YuL, XF and XW prepared the original draft of the manuscript, which they wrote, reviewed and edited. YuL and XF confirm the authenticity of all raw data. All authors reviewed and approved the final manuscript.

Ethics approval and consent to participate

The present study was approved by the ethical review committee of the Shengli Oilfield Central Hospital.

Patient consent for publication

Not applicable.

Competing interests

The authors declare that they have no competing interests.

References

1. Reid BM, Permuth JB and Sellers TA: Epidemiology of ovarian cancer: A review. Cancer Biol Med 14: 9-32, 2017.
2. Iorio MV, Visone R, Di Leva G, Donati V, Petrocca F, Casalini P, Taccioli C, Volinia S, Liu CG, Alder H, *et al*: MicroRNA signatures in human ovarian cancer. Cancer Res 67: 8699-8707, 2007.
3. Liu E, Liu Z and Zhou Y: Carboplatin-docetaxel-induced activity against ovarian cancer is dependent on up-regulated lncRNA PVT1. Int J Clin Exp Pathol 8: 3803-3810, 2015.
4. Gao Y, Meng H, Liu S, Hu J, Zhang Y, Jiao T, Liu Y, Ou J, Wang D, Yao L, *et al*: LncRNA-HOST2 regulates cell biological behaviors in epithelial ovarian cancer through a mechanism involving microRNA let-7b. Hum Mol Genet 24: 841-852, 2015.
5. Chai Y, Liu J, Zhang Z and Liu L: HuR-regulated lncRNA NEAT1 stability in tumorigenesis and progression of ovarian cancer. Cancer Med 5: 1588-1598, 2016.
6. Ganapathy-Kanniappan S: Molecular intricacies of aerobic glycolysis in cancer: Current insights into the classic metabolic phenotype. Crit Rev Biochem Mol Biol 53: 667-682, 2018.
7. Vaupel P, Schmidberger H and Mayer A: The warburg effect: Essential part of metabolic reprogramming and central contributor to cancer progression. Int J Radiat Biol 95: 912-919, 2019.
8. Yang B, Zhang L, Cao Y, Chen S, Cao J, Wu D, Chen J, Xiong H, Pan Z, Qiu F, *et al*: Overexpression of lncRNA IGFBP4-1 reprograms energy metabolism to promote lung cancer progression. Mol Cancer 16: 154, 2017.
9. Hu Y, Sun H, Hu J and Zhang X: LncRNA DLX6-AS1 promotes the progression of neuroblastoma by activating STAT2 via targeting miR-506-3p. Cancer Manag Res 12: 7451-7463, 2020.
10. Li N, Zhan X and Zhan X: The lncRNA SNHG3 regulates energy metabolism of ovarian cancer by an analysis of mitochondrial proteomes. Gynecol Oncol 150: 343-354, 2018.
11. Peng WX, Koirala P and Mo YY: LncRNA-mediated regulation of cell signaling in cancer. Oncogene 36: 5661-5667, 2017.
12. Gutschner T and Diederichs S: The hallmarks of cancer: A long non-coding RNA point of view. RNA Biol 9: 703-719, 2012.
13. Nagano T and Fraser P: No-nonsense functions for long noncoding RNAs. Cell 145: 178-181, 2011.
14. Wang M, Sun X, Yang Y and Jiao W: Long non-coding RNA OIP5-AS1 promotes proliferation of lung cancer cells and leads to poor prognosis by targeting miR-378a-3p. Thorac Cancer 9: 939-949, 2018.
15. Liu X, Zheng J, Xue Y, Yu H, Gong W, Wang P, Li Z and Liu Y: PIWIL3/OIP5-AS1/miR-367-3p/CEBPA feedback loop regulates the biological behavior of glioma cells. Theranostics 8: 1084-1105, 2018.
16. Guo L, Chen J, Liu D and Liu L: OIP5-AS1/miR-137/ZNF217 axis promotes malignant behaviors in epithelial ovarian cancer. Cancer Manag Res 12: 6707-6717, 2020.
17. Liu QY, Jiang XX, Tian HN, Guo HL, Guo H and Guo Y: Long non-coding RNA OIP5-AS1 plays an oncogenic role in ovarian cancer through targeting miR-324-3p/NFIB axis. Eur Rev Med Pharmacol Sci 24: 7266-7275, 2020.
18. Cho WC: OncomiRs: The discovery and progress of microRNAs in cancers. Mol Cancer 6: 60, 2007.
19. Gregory RI and Shiekhattar R: MicroRNA biogenesis and cancer. Cancer Res 65: 3509-3512, 2005.
20. Chen J, Zhao D and Meng Q: Knockdown of HCP5 exerts tumor-suppressive functions by up-regulating tumor suppressor miR-128-3p in anaplastic thyroid cancer. Biomed Pharmacother 116: 108966, 2019.
21. Zhao J, Li D and Fang L: MiR-128-3p suppresses breast cancer cellular progression via targeting LIMK1. Biomed Pharmacother 115: 108947, 2019.
22. Zhang C, Xie L, Liang H and Cui Y: LncRNA MIAT facilitates osteosarcoma progression by regulating mir-128-3p/VEGFC axis. IUBMB Life 71: 845-853, 2019.
23. Xu M, Zhou K, Wu Y, Wang L and Lu S: Linc0a0161 regulated the drug resistance of ovarian cancer by sponging microRNA-128 and modulating MAPK1. Mol Carcinog 58: 577-587, 2019.
24. Li R, Gong L, Li P, Wang J and Bi L: MicroRNA-128/homeobox B8 axis regulates ovarian cancer cell progression. Basic Clin Pharmacol Toxicol 125: 499-507, 2019.

25. Baek WK, Kim D, Jung N, Yi YW, Kim JM, Cha SD, Bae I and Cho CH: Increased expression of cyclin G1 in leiomyoma compared with normal myometrium. Am J Obstet Gynecol 188: 634-639, 2003.
26. Perez R, Wu N, Klipfel AA and Beart RW Jr: A better cell cycle target for gene therapy of colorectal cancer: Cyclin G. Gastroenterology 7: 884-889, 2003.
27. Gramantieri L, Ferracin M, Fornari F, Veronese A, Sabbioni S, Liu CG, Calin GA, Giovannini C, Ferrazzi E, Grazi GL, *et al*: Cyclin G1 is a target of miR-122a, a microRNA frequently down-regulated in human hepatocellular carcinoma. Cancer Res 67: 6092-6099, 2007.
28. Liu X, Ma L, Rao Q, Mao Y, Xin Y, Xu H, Li C and Wang X: MiR-1271 inhibits ovarian cancer growth by targeting cyclin G1. Med Sci Monit 21: 3152-3158, 2015.
29. Yan J, Jiang JY, Meng XN, Xiu YL and Zong ZH: MiR-23b targets cyclin G1 and suppresses ovarian cancer tumorigenesis and progression. J Exp Clin Cancer Res 35: 31, 2016.
30. Livak KJ and Schmittgen TD: Analysis of relative gene expression data using real-time quantitative PCR and the 2(-Delta Delta C(T)) method. Methods 25: 402-408, 2001.
31. Albright JL: Dairy animal welfare: Current and needed research. J Dairy Sci 70: 2711-2731, 1987.
32. Swearengen JR: Common challenges in safety: A review and analysis of AAALAC findings. ILAR J 59: 127-133, 2018.
33. Lou W, Ding B and Fu P: Pseudogene-derived lncRNAs and their miRNA sponging mechanism in human cancer. Front Cell Dev Biol 8: 85, 2020.
34. Wu DD, Chen X, Sun KX, Wang LL, Chen S and Zhao Y: Role of the lncRNA ABHD11-AS1 in the tumorigenesis and progression of epithelial ovarian cancer through targeted regulation of RhoC. Mol Cancer 16: 138, 2017.
35. Zhu FF, Zheng FY, Wang HO, Zheng JJ and Zhang Q: Downregulation of lncRNA TUBA4B is associated with poor prognosis for epithelial ovarian cancer. Pathol Oncol Res 24: 419-425, 2018.
36. Arunkumar G, Anand S, Raksha P, Dhamodharan S, Prasanna Srinivasa Rao H, Subbiah S, Murugan AK and Munirajan AK: LncRNA OIP5-AS1 is overexpressed in undifferentiated oral tumors and integrated analysis identifies as a downstream effector of stemness-associated transcription factors. Sci Rep 8: 7018, 2018.
37. Hu GW, Wu L, Kuang W, Chen Y, Zhu XG, Guo H and Lang HL: Knockdown of linc-OIP5 inhibits proliferation and migration of glioma cells through down-regulation of YAP-NOTCH signaling pathway. Gene 610: 24-31, 2017.
38. Naemura M, Kuroki M, Tsunoda T, Arikawa N, Sawata Y, Shirasawa S and Kotake Y: The long noncoding RNA OIP5-AS1 is involved in the regulation of cell proliferation. Anticancer Res 38: 77-81, 2018.
39. Bai Y and Li S: Long noncoding RNA OIP5-AS1 aggravates cell proliferation, migration in gastric cancer by epigenetically silencing NLRP6 expression via binding EZH2. J Cell Biochem 121: 353-362, 2020.
40. Sen R, Ghosal S, Das S, Balti S and Chakrabarti J: Competing endogenous RNA: The key to posttranscriptional regulation. Sci World J 2014: 896206, 2014.
41. Tan JY, Sirey T, Honti F, Graham B, Piovesan A, Merkenschlager M, Webber C, Ponting CP and Marques AC: Extensive microRNA-mediated crosstalk between lncRNAs and mRNAs in mouse embryonic stem cells. Genome Res 25: 655-666, 2015.
42. Sui J, Li YH, Zhang YQ, Li CY, Shen X, Yao WZ, Peng H, Hong WW, Yin LH, Pu YP and Liang GY: Integrated analysis of long non-coding RNA-associated ceRNA network reveals potential lncRNA biomarkers in human lung adenocarcinoma. Int J Oncol 49: 2023-2036, 2016.
43. Sun WL, Kang T, Wang YY, Sun JP, Li C, Liu HJ, Yang Y and Jiao BH: Long noncoding RNA OIP5-AS1 targets Wnt-7b to affect glioma progression via modulation of miR-410. Biosci Rep 39: BSR20180395, 2019.
44. Escoté X and Fajas L: Metabolic adaptation to cancer growth: From the cell to the organism. Cancer Lett 356: 171-175, 2015.
45. Icard P, Fournel L, Wu Z, Alifano M and Lincet H: Interconnection between metabolism and cell cycle in cancer. Trends Biochem Sci 44: 490-501, 2019.
46. Horne MC, Goolsby GL, Donaldson KL, Tran D, Neubauer M and Wahl AF: Cyclin G1 and cyclin G2 comprise a new family of cyclins with contrasting tissue-specific and cell cycle-regulated expression. J Biol Chem 271: 6050-6061, 1996.
47. Jensen MR, Factor VM, Fantozzi A, Helin K, Huh CG and Thorgeirsson SS: Reduced hepatic tumor incidence in cyclin G1-deficient mice. Hepatology 37: 862-870, 2003.